Simulation of mineral solid solutions at zero and high pressure using lattice statics, lattice dynamics and Monte Carlo methods

2004 J. Phys.: Condens. Matter 16 S2751

(http://iopscience.iop.org/0953-8984/16/27/011)

INSTITUTE OF PHYSICS PUBLISHING JOURNAL OF PHYSICS: CONDENSED MATTER

J. Phys.: Condens. Matter **16** (2004) S2751–S2770 PII: S0953-8984(04)70572-X

Simulation of mineral solid solutions at zero and high pressure using lattice statics, lattice dynamics and Monte Carlo methods

I T Todorov[1], N L Allan[1], M Yu Lavrentiev[1,4], C L Freeman[1], C E Mohn[2] and J A Purton[3]

[1] School of Chemistry, University of Bristol, Cantock's Close, Bristol BS8 1TS, UK
[2] Department of Chemistry, University of Oslo, Postbox 1033 Blindern, N0315 Oslo, Norway
[3] CLRC, Daresbury Laboratory, Warrington, Cheshire WA4 4AD, UK

E-mail: n.l.allan@bris.ac.uk

Received 15 October 2003
Published 25 June 2004
Online at stacks.iop.org/JPhysCM/16/S2751
doi:10.1088/0953-8984/16/27/011

Abstract

We discuss how two techniques, based on (1) lattice statics/lattice dynamics simulations and (2) Monte Carlo methods may be used to calculate the thermodynamic properties of oxide mixtures at zero and high pressure. The lattice statics/lattice dynamics calculations involve a full free energy structural optimization of each of a number of configurations, followed by thermodynamic averaging. Strategies for generating a suitable set of configurations are discussed. We compare results obtained by random generation with those obtained using radial distribution functions or explicit symmetry arguments to obtain approximate or exact weightings respectively for individual configurations. The Monte Carlo simulations include the explicit interchange of cations and use the semigrand canonical ensemble for chemical potential differences. Both methods are readily applied to high pressures and elevated temperatures without the need for any new parametrization. Agreement between the two techniques is better at high pressures where anharmonic terms are smaller. We compare in detail the use of each technique for properties such as enthalpies, entropies, volume and free energies of mixing at zero and high pressure and thus calculation of the phase diagram. We assess the vibrational contributions to these quantities and compare results with those in the dilute limit. The techniques are illustrated throughout using MnO–MgO and should be readily applicable to more complicated systems.

(Some figures in this article are in colour only in the electronic version)

[4] On leave from: Institute of Inorganic Chemistry, 630090 Novosibirsk, Russia.

1. Introduction

Grossly disordered minerals and non-ideal solid solutions, particularly of oxides, continue to present considerable challenges to the theoretician. The cluster variation method (CVM) [1], for example, widely used for metallic alloys, often performs poorly where species involved are markedly dissimilar, as is usually the case in ceramics and minerals. In addition, the use of parametrized Hamiltonians (e.g., of Ising type) is increasingly difficult beyond binary or pseudobinary alloys. Disorder in ionic materials has chiefly been studied via point defect calculations [2] (the dilute limit), with the first general-purpose code (HADES) pioneered by Norgett in the early 1970s [3]. Another route has been via the use of a 'supercell' [4], in which a periodic 'superlattice' of defects is introduced, extending throughout the macroscopic crystal; an artificial ordering is thus imposed on the arrangement of defects by the periodic boundary conditions. In this paper we discuss two multi-configuration techniques for solid solutions or disordered systems with a *finite* impurity or defect content far from the dilute limit. Both of these, unlike the point defect or supercell calculations, sample many different arrangements of ions. Both are readily applied to high pressure and include thermal (vibrational) effects, which have proved problematic for traditional methods [1].

The first of these builds on a highly efficient method for the fully dynamic structure optimization of large unit cells which uses lattice statics and quasiharmonic lattice dynamics (QLD). The accurate calculation of the free energy via QLD is quick and computationally efficient and does not resort to lengthy thermodynamic integration. The full set of free energy first derivatives is calculated analytically and a minimization of the free energy with respect to all structural variables for large unit cells is possible [5, 6]. Here this technique is extended to evaluate the *free energies* of solid solutions (including ΔH_{mix}, ΔS_{mix}) and phase diagrams at *any* pressure. This is achieved by forming a thermodynamic average of the free energies of a number of configurations. We pay particular attention to the problem of how to choose these configurations. No *a priori* assumptions are made regarding the configurational entropy contribution and the vibrational contributions to thermodynamic quantities at any temperature and pressure are determined straightforwardly.

The configurationally averaging differs in some important respects from CVM [7]. This defines the energy of the system as an expansion of effective cluster interactions (ECIs). These ECIs are calculated by fitting to the energy of several configurations. A large range of further configurations can then be generated by applying the ECIs within the configuration to calculate their energy. This method differs significantly from ours where all configurations are relaxed. Each possible arrangement is not specifically optimized in CVM. Zunger *et al* [8] have suggested the use of a special quasirandom structure (SQS) which mimics the properties of the ensemble average. Where the interactions within the system are complex or long range the number of ECIs that need to be defined in the CVM can make the expansion unfeasible [9]. Perovskites [10], for example, have proved problematic while application to carbonates [11] has required an extremely time-consuming procedure for fitting.

The second technique is the well-known Monte Carlo method, extended in such a way that *both* the atomic configuration *and* the atomic coordinates of all the atoms are changed. We denote this approach as Monte Carlo exchange (MCX). While absolute values of the free energy cannot be obtained readily from Monte Carlo simulations, the semigrand canonical ensemble [12, 13] provides a convenient route to accurate chemical potential *differences* accurately and hence the phase diagram. Simulations using this ensemble have been carried out for liquids and alloys [14] but, to our knowledge, the technique remains unexplored for minerals.

We illustrate the methods throughout using the binary system MnO–MgO as an example, a convenient choice for our purpose due to the mismatch in size between the two cations.

While the emphasis in this paper is on the methodology, it is worth mentioning the conflicting reports of the phase diagram of this system. As shown in [15], the experiments of Raghavan *et al* [16] suggest a consolute temperature, T_c, as low as 600 K, whereas the results of Wood *et al* [17] are consistent with a much larger T_c ($\approx$1100 K) and a markedly asymmetric phase diagram. The data of [16] are surprising bearing in mind the large two-phase region in the CaO–MgO phase diagram, and the difference in ionic radius between Mn^{2+} and Mg^{2+}, which is substantial although smaller than between Ca^{2+} and Mg^{2+}.

The structure of this paper is as follows. We first summarize the main features of the configurational averaging via QLD and Monte Carlo methods. A wide range of thermodynamic properties at zero pressure are then considered, including, for example, enthalpies, entropies, Gibbs energies and volumes of mixing, and results from the two methods are compared in detail. We then present results at high pressure (50 GPa). Finally we return to consider the configurational averaging technique in detail and the problem of choice of configuration, classifying configurations via their radial distribution function or space group symmetry.

2. Thermodynamics of solid solutions: theoretical methods

2.1. Lattice statics and dynamics

In principle a solid solution can assume any state in which each atom can be at any position. The only states of practical importance away from the melting point will lie at the bottom of K local minima in the energy of the system, i.e., they correspond to a given configuration. For each configuration k, we suppose there are a number of states which correspond to small or moderate changes in the internal and external lattice strains. States corresponding to large changes in these strains have high energies and do not contribute significantly to the equilibrium properties of the system. These are ignored. Using the label $k = 1, \ldots, K$ for the configuration, then the enthalpy and Gibbs energy in the isobaric–isothermal (NPT) ensemble are given by [18]

$$H = \frac{\sum_{k=1}^{K} H_k \exp(-G_k/k_B T)}{\sum_{k=1}^{K} \exp(-G_k/k_B T)}, \tag{1}$$

$$G = -k_B T \ln \sum_{k=1}^{K} \exp(-G_k/k_B T) \tag{2}$$

where k_B is Boltzmann's constant. G_k is the Gibbs energy for the relaxed structure of each possible cation arrangement. We thus have expressions for any thermodynamic quantity in terms of quantities obtained with particular configurations. The thermodynamic averaging is performed over the results of a set of full free energy minimizations of different arrangements (configurations) of the cations within a supercell.

It is useful to rewrite G as

$$G = -k_B T \ln K - k_B T \ln\left(\sum_{k=1}^{K} \exp(-G_k/k_B T)/K\right) \tag{3}$$

where K is the total number of possible configurations for the supercell considered. The first term in equation (3) is the ideal term, and the second the deviation from ideality. For other than the smallest supercells it is impractical to sum over all K configurations and all summations in equations (1) and (2) are restricted to K' configurations chosen at random; K in the second term of equation (3) is replaced by K'. Thus

$$H = \frac{\sum_{k=1}^{K'} H_k \exp(-G_k/k_B T)}{\sum_{k=1}^{K'} \exp(-G_k/k_B T)}, \tag{4}$$

and

$$G = -k_{\mathrm{B}}T \ln K - k_{\mathrm{B}}T \ln\left(\sum_{k=1}^{K'} \exp(-G_k/k_{\mathrm{B}}T)/K'\right). \tag{5}$$

We show later convergence in both these quantities can be reached using a manageable value of K'. The entropy is readily obtained from $(H - G)/T$. The minimizations of the free energies of individual configurations are all carried out with the code SHELL [5].

The volume is given by an equation analogous to equation (4);

$$V = \frac{\sum_{k=1}^{K} V_k \exp(-G_k/k_{\mathrm{B}}T)}{\sum_{k=1}^{K} \exp(-G_k/k_{\mathrm{B}}T)}, \tag{6}$$

where V_k is the volume of configuration k.

2.2. Monte Carlo simulations

The Monte Carlo exchange simulations (MCX) have been described previously [19, 20]. These are carried out within the NPT ensemble, i.e., both the atomic coordinates and cell dimensions are allowed to vary during the simulation. Randomly selected atoms are moved at random in order to take vibrational effects into account. In any step, a random choice is made whether to attempt a random exchange between two atoms, a random displacement of an ion, or a random change in the volume of the simulation box. To determine whether the change is accepted or rejected, the usual Metropolis algorithm [21] is applied. The maximum changes in the atomic displacements and the lattice parameters are governed by the variables $r_{\max}$ and $v_{\max}$ respectively, and these are adjusted automatically during the equilibration part of the simulation to maintain an acceptance ratio of approximately 0.3. Calculation of the free energy is less straightforward than with QLD; semigrand canonical ensemble simulations are used to calculate the difference in chemical potential of Mg and Mn ions. The conversion of one species, B into another, A, is considered, and the resulting potential energy change $\Delta U_{\mathrm{B/A}}$ determined. This is related to the change in chemical potential $\Delta\mu_{\mathrm{B/A}}$ by

$$\Delta\mu_{\mathrm{B/A}} = -k_{\mathrm{B}}T \ln\left\langle \frac{N_{\mathrm{B}}}{N_{\mathrm{A}} + 1} \exp(-\Delta U_{\mathrm{B/A}}/k_{\mathrm{B}}T)\right\rangle. \tag{7}$$

Every fifth step (on average) of the MCX simulation we evaluate the energy associated with the conversion of a randomly chosen Mg^{2+} ion to Mn^{2+}, $\Delta U_{\mathrm{Mg/Mn}}$, and as the simulation proceeds the average value of the exponential in equation (7) is determined. Note that the change of Mg^{2+} into Mn^{2+} is *not* actually performed since the configuration remains unchanged after evaluating $\Delta U_{\mathrm{Mg/Mn}}$, and that it is important to check consistency, i.e., here that identical results are obtained considering the reverse transformation, i.e., of a randomly chosen Mn^{2+} to a Mg^{2+}.

All calculations in this paper are based on a rigid ion model using two-body potentials, taken from [22] to represent non-Coulombic interactions between the ions. In a few places, where stated, we have also used the shell model [23] to allow for ionic polarization.

3. Thermodynamic properties at zero pressure

We start with results from QLD. Figure 1 shows values of the calculated enthalpy of mixing, ΔH_{mix}, for a 50/50 mixture of MnO and MgO[5] at 1000 K as a function of supercell size

[5] For the 54-atom cell the 50/50 results are an arithmetic mean of those for cells containing 13Mn/14Mg and 14Mn/13Mg. All the results for these two compositions are indistinguishable on the scale of the graphs plotted in this paper.

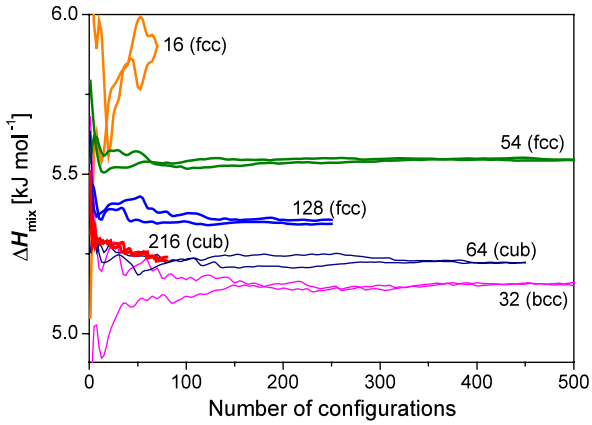

Figure 1. Calculated values of ΔH_{mix} (kJ mol^{-1}) for a 50/50 MnO–MgO composition at 1000 K as a function of supercell size and number of configurations. The number attached to each curve denotes the total number of atoms in each supercell and fcc, bcc and cub denote face-centred cubic, body-centred cubic and cubic supercell symmetries respectively.

and number of (fully optimized) configurations, determined using equations (1) or (4) as appropriate. All external and internal degrees of freedom are optimized for every configuration. For a (cubic) 8-atom unit cell all six configurations for this composition are symmetrically equivalent, and the resulting enthalpy of mixing is so high (8.8 kJ mol^{-1}) that it is not included in the plot. For all the cell sizes considered in figure 1, results for two different sets of randomly chosen configurations are shown. For a 16-atom cell there are 70 configurations for the 50/50 composition. The *small* number of configurations required for convergence is striking. For the 32 cell satisfactory convergence in ΔH_{mix} (to 0.04 kJ mol^{-1}) with number of configurations is typically obtained with only ≈150 out of a total of 12 870 configurations. To confirm the value of ΔH_{mix} for this cell, we have optimized *all* 12 870 arrangements and the resulting value is unchanged from the value obtained with 150. Larger cells, for which the total number of configurations is much larger (e.g., 2×10^7 for a 54-ion cell), need not more than 100 configurations for satisfactory convergence of ΔH_{mix}. Very similar results are obtained when the supercell is constrained to remain cubic during the optimization of each configuration.

Convergence in ΔH_{mix} with respect to cell size is obtained with relatively small cells. The trend is easier to see in figure 2, where values of ΔH_{mix} are plotted as a function of $1/N$, where N is the total number of ions in the supercell. Each set of supercells with the same superlattice type (face-centred, simple cubic or body-centred cubic) converge at a different rate. As with point defect supercell calculations for MgO [4], face-centred cells appear to converge fastest. For example, the difference in the value of ΔH_{mix} obtained using a 54-atom cell and that obtained by extrapolation to infinite cell size is only ≈0.2 kJ mol^{-1}.

Shown in figure 3 are values of ΔH_{mix} at 1000 K and zero pressure obtained with MCX, using a simulation cell of 512 ions, and 4×10^7 steps, following initial equilibration of 1×10^7 steps. The plot shows there is good agreement between QLD and MCX[6], despite QLD using vastly less configurations than MCX and neglecting higher-order anharmonic terms (though quantum effects are incorporated in QLD). The calculated ΔH_{mix} at 1000 K is symmetric with a maximum of 5.4 kJ mol^{-1}. *No* symmetry constraints are applied in any of the calculations.

[6] In contrast MC simulations, without cation exchanges, show a strong variation of over 1 kJ mol^{-1} with the choice of initial arrangement.

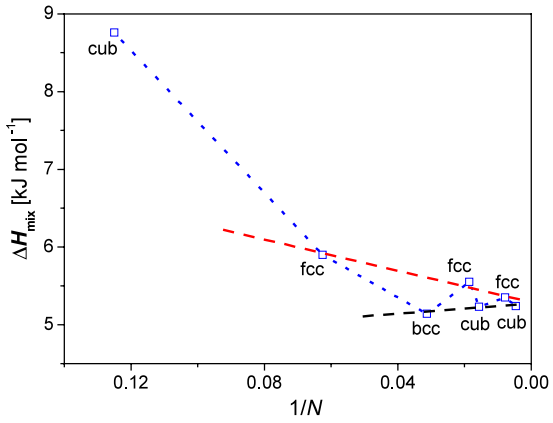

Figure 2. ΔH_{mix} (kJ mol^{-1}) at 1000 K for a 50/50 MnO–MgO composition versus $1/N$ where N is the total number of atoms in the supercell.

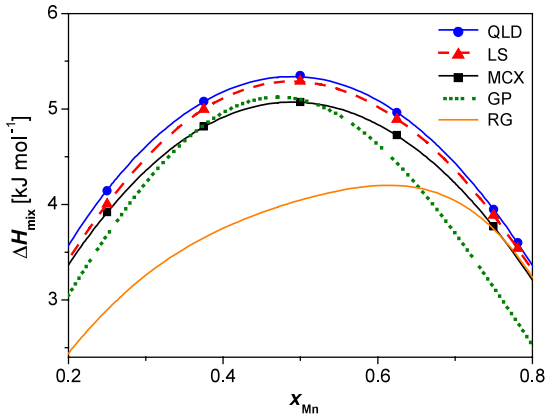

Figure 3. ΔH_{mix} (kJ mol^{-1}) at 1000 K for MnO–MgO as a function of composition calculated using configurational quasiharmonic lattice dynamics (QLD) and using exchange Monte Carlo (MCX). LS denotes values calculated using configurational averaging but with each configuration minimized in the static limit, using lattice statics (rather than a full free energy minimization), as described in the text. Two sets of experimental data (GP [24], RG [25]) are shown.

Agreement with [24] is satisfactory; the results do not show the asymmetry reported in [25]. We have discussed previously [18] the striking failure of mean-field approach and 'hybrid' potentials for ΔH_{mix}. Figure 4 shows the variation of ΔH_{mix} for the 50/50 mixture with temperature, calculated using QLD and the 128-ion cell. Results from MCX are very similar, indicating that ΔH_{mix} varies only slightly with temperature.

The volume of mixing, ΔV_{mix}, calculated via equation (6) converges more rapidly with number of randomly chosen configurations than any other property considered in this paper. For supercells with more than 16 ions less than 50 configurations are needed for satisfactory convergence in ΔV_{mix} to 10^{-9} m^3 mol^{-1}. Figure 5 shows a plot of ΔV_{mix} with composition, obtained from both QLD and MCX. The values are small and negative with a displacement of the minimum away from the 50–50 composition towards a higher Mg content. There is a larger difference between the MCX and QLD values than for ΔH_{mix}; both methods indicate that ΔV_{mix} increases with temperature, with QLD indicating a larger variation than MCX.

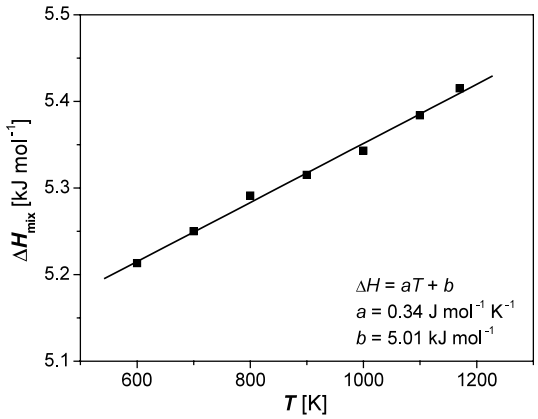

Figure 4. The variation of $\Delta H_{\rm mix}$ (kJ mol^{-1}) for the 50/50 MnO–MgO mixture with temperature (QLD results for the 128-ion supercell).

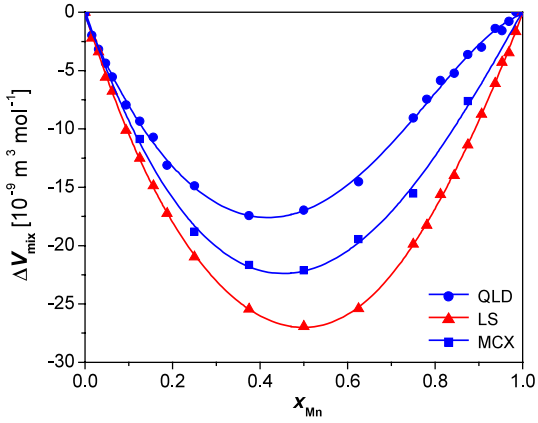

Figure 5. The variation of $\Delta V_{\rm mix}$ (10^{-9} m^3 mol^{-1}) for MnO–MgO with composition. The results from configurational quasiharmonic lattice dynamics (QLD), exchange Monte Carlo (MCX) and configurational averaging using the results of lattice statics minimizations (LS) are compared.

We turn to entropies of mixing, $\Delta S_{\rm mix}$, calculated using QLD. In figure 6(a), $\Delta S_{\rm mix}$, for the 50/50 composition at 1000 K is plotted as a function of number of configurations. As in figure 1, results for two different sets of randomly chosen configurations are shown for each cell size. As with $\Delta H_{\rm mix}$ and $\Delta V_{\rm mix}$, $\Delta S_{\rm mix}$ converges with number of configurations for every cell size. Supercells with more than 16 atoms require no more than 150 configurations for satisfactory convergence of $\Delta S_{\rm mix}$ (to 0.02 J mol^{-1} K^{-1}). The convergence of $\Delta S_{\rm mix}$ with cell size, shown in figure 6(b), is somewhat slower than that of $\Delta H_{\rm mix}$. For example, the difference in the value of $\Delta S_{\rm mix}$ obtained using a 54-atom cell and that obtained by extrapolation to infinite cell size is $\approx$0.5 J K^{-1} mol^{-1}. We stress that $\Delta S_{\rm mix}$ includes *both* configurational *and* vibrational contributions. The solid line in this figure indicates the ideal (bulk) entropy of mixing for this composition (5.78 J mol^{-1} K^{-1}). The excess $\Delta S_{\rm mix}$ is negative for smaller cells (<64 ions), but changes sign for larger cells. We return to consider the configurational and vibrational contributions in more detail in the next section. Figure 6(c) plots $\Delta S_{\rm mix}$ as a function of composition at 1000 K. $\Delta S_{\rm mix}$ is larger than the ideal value for compositions

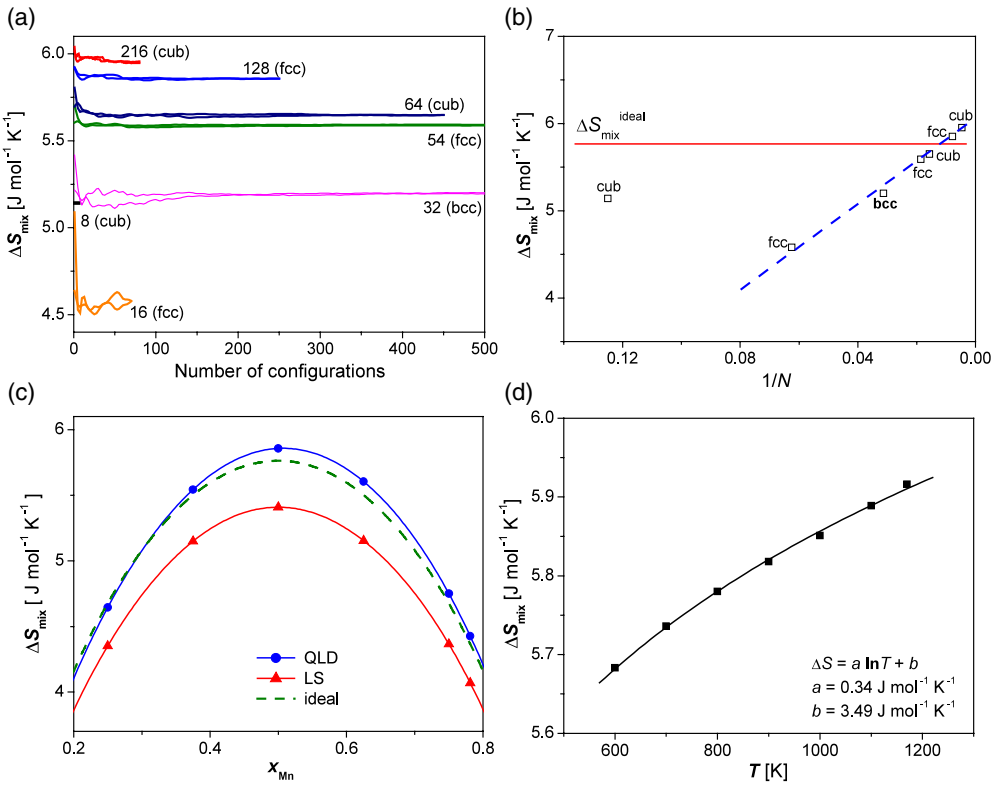

Figure 6. (a) Values of ΔS_{mix} (J K^{-1} mol^{-1}) at 1000 K for a 50/50 MnO–MgO composition as a function of supercell size and number of configurations. The number attached to each curve denotes the total number of atoms in each supercell and fcc, bcc and cub denote face-centred cubic, body-centred cubic and cubic supercell symmetries respectively. (b) ΔS_{mix} (J K^{-1} mol^{-1}) at 1000 K for a 50/50 MnO–MgO composition versus $1/N$ where N is the total number of atoms in the supercell. (c) ΔS_{mix} (J K^{-1} mol^{-1}) at 1000 K for MnO–MgO as a function of composition calculated using configurational quasiharmonic lattice dynamics (QLD) (filled circles). The points (hollow circles) labelled LS are values calculated using configurational averaging but with each configuration minimized in the static limit, using lattice statics (rather than a full free energy minimization), as described in the text. For comparison the ideal entropy of mixing is also shown (dashed curve). (d) The variation of ΔS_{mix} (J K^{-1} mol^{-1}) for the 50/50 MnO–MgO mixture with temperature (QLD results for the 128-ion supercell).

with $x_{\mathrm{Mn}} > \approx 0.3$ (ideal entropies of mixing of course do not include vibrational terms). Figure 6(d) shows the small variation of ΔS_{mix} with temperature for the 50/50 composition; below 800 K ΔS_{mix} is lower than the ideal value, reflecting the tendency for cluster formation and incomplete random mixing at lower temperatures.

The calculation of the free energy of mixing is a severe test of our model since ΔH_{mix} and $-T\,\Delta S_{\mathrm{mix}}$ are often very close in magnitude. This is illustrated for the 50/50 composition in figures 7(a) and (b), which show that larger cell sizes and a greater number of configurations are required for convergence. For the 32- and 128-atom supercells, for example, 250 and 100 configurations are required respectively for convergence (with number of configurations) to less than 0.04 kJ mol^{-1}. The difference in the value of ΔG_{mix} obtained using a 54-atom cell and that obtained by extrapolation to infinite cell size is ≈ -0.8 kJ mol^{-1}. Nevertheless for MnO–MgO 250 configurations with a supercell of 128 atoms are sufficient to ensure adequate

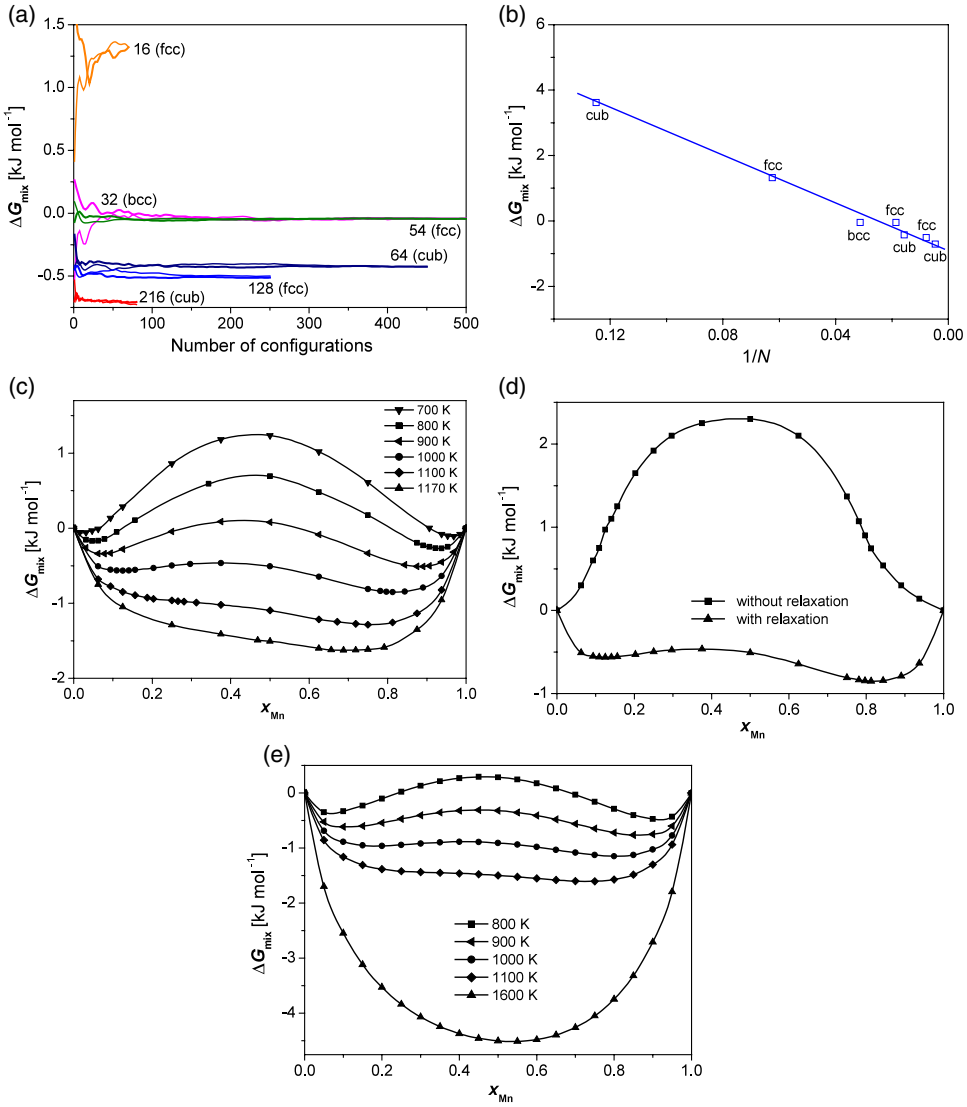

Figure 7. (a) Calculated values of ΔG_{mix} (kJ mol^{-1}) for a 50/50 MnO–MgO composition at 1000 K as a function of supercell size and number of configurations. The number attached to each curve denotes the total number of atoms in each supercell and fcc, bcc and cub denote face-centred cubic, body-centred cubic and cubic supercell symmetries respectively. (b) ΔG_{mix} (kJ mol^{-1}) at 1000 K for a 50/50 MnO–MgO composition versus $1/N$ where N is the total number of atoms in the supercell. (c) Variation of ΔG_{mix} (kJ mol^{-1}) for MnO–MgO with composition. The results are calculated for a range of temperatures using configurational quasiharmonic lattice dynamics QLD. (d) Demonstration of the importance of atomic relaxation. The variations of ΔG_{mix} (kJ mol^{-1}) at 1000 K for MnO–MgO with composition, with and without relaxation are plotted. All calculations configurational quasiharmonic lattice dynamics. (e) Variation of ΔG_{mix} (kJ mol^{-1}) for MnO–MgO with composition. The results are calculated for a range of temperatures using exchange Monte Carlo (MCX).

convergence in the positions of the two minima in the ΔG_{mix} versus composition curves in figure 7(c) which plots ΔG_{mix} versus x_{Mn} for this cell size over a wide range of temperatures. The *vital* importance of allowing for atomic relaxation is shown strikingly in figure 7(d) which

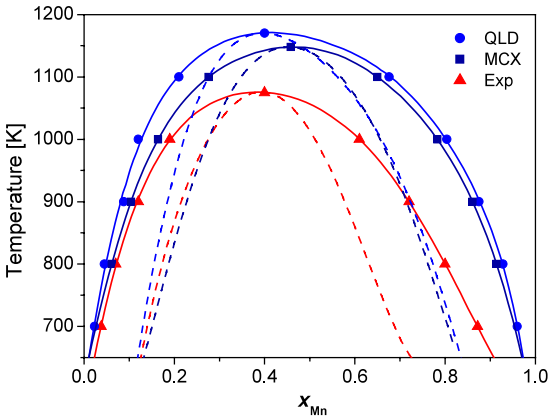

Figure 8. Phase diagrams for MnO–MgO at zero pressure calculated using QLD (circles), MCX (squares), and from experiment [15] (triangles). Spinodals are also shown (dashed curves).

compares calculated ΔG_{mix} versus composition curves at 1000 K with and without relaxation. In the absence of relaxation ΔG_{mix} is *positive* for all compositions studied in this system, which illustrates, dramatically, the importance of relaxation.

Monte Carlo simulations at a given temperature in the semigrand canonical ensemble yield the calculated variation of $\Delta\mu_{\mathrm{Mg/Mn}}$ with composition. As in the Margules approximation [26], we write the excess (non-ideal) free energy as a third-degree polynomial in the concentration:

$$G_{\mathrm{excess}} = (W_1 x_2 + W_2 x_1) x_1 x_2 \tag{8}$$

where x_1 and x_2 are the mole fractions of the components and the W are asymmetric interaction parameters: W_1, for example, is the energy of putting component 1 into component 2, and vice versa. The chemical potential difference then consists of an ideal solution term and a second-degree polynomial:

$$\frac{\Delta\mu}{k_{\mathrm{B}}T} = \frac{\Delta\mu_0}{k_{\mathrm{B}}T} + \ln\left(\frac{x_1}{x_2}\right) + W_1 x_2(1 - 3x_1) - W_2 x_1(1 - 3x_2). \tag{9}$$

The results for $\Delta\mu$ at each temperature were fitted to a curve of the form of equation (9). Integration then gives the variation of free energy with composition, and the resulting ΔG_{mix} versus composition curves are shown in figure 7(e). These curves are similar to those obtained in figure 7(c) using QLD. There is also good agreement between ΔS_{mix} values obtained via the Monte Carlo free energy and enthalpy of mixing and those obtained from QLD.

Common tangent constructions to the data in figures 7(c) and (e) yield the calculated phase diagrams and spinodals in figure 8. Also shown in the figure are those obtained by de Villiers *et al* [15] using the experimental data of [17]. The agreement between the QLD and MCX simulations is good, and our results provide strong support for the experimental results of Wood *et al* [17], ruling out the formation of a complete solid solution at temperatures as low as 600 K, as suggested in [16]. The calculated phase diagram possesses a marked asymmetry with MnO less soluble in MgO than MgO in MnO. The same type of asymmetry is also observed in the CaO/MgO system, with the smaller cation more soluble in CaO than the larger cation in MgO. The phase diagram obtained from the measurements of Wood *et al* [17] is more asymmetric than those calculated. de Villiers *et al* [15] have discussed the experimental errors and conclude this asymmetry should be smaller.

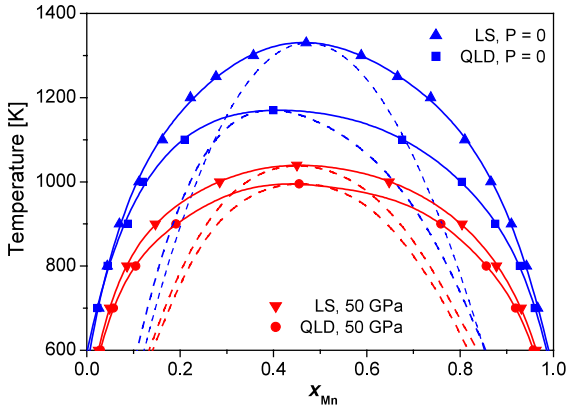

Figure 9. Calculated phase diagrams for MnO–MgO at 0 and 50 GPa calculated using QLD and LS configurational averaging. Spinodals are also shown (dashed curves).

3.1. Vibrational contributions and the 'lattice statics' approximation

All the calculations in the previous section involved the full free energy minimization of each configuration. It is computationally much cheaper to optimize every configuration in the static limit, using lattice statics (LS). When we refer below to LS values or, equivalently, thermodynamic properties of the solid solutions in the static limit, configurationally averaged values are evaluated using equations (1)–(5) replacing G_k with H_k (static). The vibrational contribution to H_k and the vibrational entropy S_k are ignored. Not only is the minimization of each configuration much cheaper but in addition only *one* set of runs over the composition scale is required for *all* temperatures.

The curves labelled LS in figures 3, 5, and 6(c) show, in turn, $\Delta H_{\rm mix}$, $\Delta V_{\rm mix}$ and $\Delta S_{\rm mix}$ calculated using this approximation. All the curves show the same qualitative features as those obtained using the full minimizations. An important further advantage of this comparison is the ability to assess the vibrational contributions to each thermodynamic property. The difference between the QLD and LS values represent this vibrational contribution (denoted using the subscript 'vib'). LS values of $\Delta H_{\rm mix}$ are slightly smaller than the dynamic values. The vibrational contributions are positive with a maximum of $\approx$0.16 kJ mol^{-1} at $x_{\rm Mn} \approx 0.5$. The vibrational contributions to $\Delta V_{\rm mix}$ are also positive, with the LS values more negative and more symmetric about $x_{\rm Mn} = 0.5$ than the full curve.

Neglecting effects due to thermal expansion, the LS values of $\Delta S_{\rm mix}$ represent the configurational contribution to this quantity (denoted by the subscript 'config' below). The LS values of $\Delta S_{\rm mix}$ are lower and smaller than the ideal entropy of mixing at all compositions. $\Delta S_{\rm mix(config)}$ is thus smaller than the ideal, suggesting the mixing is not completely random. As we seen the total $\Delta S_{\rm mix}$ is larger than the ideal value. This is due to positive vibrational entropy terms. The maximum contribution of $\Delta S^{\rm vibr}_{\rm mix}$ at 1000 K is 8% of the total $\Delta S_{\rm mix}$ for $x_{\rm Mn} = 0.5$.

Figure 9 shows the calculated phase diagram obtained using LS values of $\Delta G_{\rm mix}$. The diagram is broadly similar to that obtained using the full dynamic free energies (figure 8), but the consolute temperature is 160 K larger (an increase of $\approx$14%) and the corresponding value of $x_{\rm Mn}$ closer to 0.5.

To assess the likely effects of the thermal expansion of the lattice, we have used the ZSISA approximation [27] and carried out static limit minimizations, analogous to those just described, at the volumes suggested for each configuration by the fully dynamic optimizations.

This volume is kept fixed during the static optimization. The results of these calculations are virtually indistinguishable from the full minimization.

3.2. Finite concentrations versus the point defect limit

Since traditionally most calculations relating to the incorporation of trace elements or impurities in oxides have concentrated on the dilute limit, it is of interest to compare computed properties at finite concentration with those predicted from calculations in the point defect limit. As an example we consider the entropy. Point defect entropies, s_p, of substitution at constant pressure are given by

$$s_p = s_p(P, T) = \{S_{dc}(P, T) - S_{pc}(P, T)\}/N_d \tag{10}$$

where S_{dc} and S_{pc} are the entropies of the microscopic defect crystal and perfect crystal, respectively, and N_d is the total number of defects introduced into the microscopic crystal. s_p can be calculated as described previously in [4] using a supercell of pure MgO or MnO containing 128 cations and the same cell (fully optimized) in which one cation is replaced by a Mn^{2+} or Mg^{2+} respectively. Note there is no configurational entropy contribution to s_p, which arises entirely from differences in vibrational frequencies between the pure and defective supercells. Convergence towards properties of an isolated defect occurs as the superlattice spacing is increased and a suitable extrapolation procedure is discussed in [4].

The point defect entropy at constant pressure, s_p of a Mn^{2+} substitutional defect in MgO or a Mg^{2+} defect in MnO, was calculated using a large supercell (here 216 ions), using the method described in [4]. When a Mg^{2+} ion in MgO is replaced by Mn^{2+}, s_p is $\approx$18.4 J K^{-1} mol^{-1} at 1000 K. This vibrational contribution is positive since it is dominated by the heavier Mn^{2+} and the expansion of the lattice it produces, both of which decrease frequencies. Conversely when a Mn^{2+} ion in MnO is replaced by Mg^{2+}, s_p is negative (≈ -14.8 J mol^{-1} K^{-1} at 1000 K). We can use these values to estimate vibrational contributions to ΔS_{mix} assuming the dilute limit quantities do not change with composition. Figure 10 plots ΔS_{mix}^{vibr} determined using this approximation and for comparison plots the values obtained from the difference of the QLD and LS simulations as described above. It is clear that the point defect calculations are of limited use between $x_{Mn} = 0.2$ and 0.8; in the middle of the composition range they overestimate the vibrational contribution. A cheap approximation to the vibrational contribution at *any* composition is the evaluation of the vibrational entropy of the lowest energy configuration. Values of ΔS_{mix}^{vibr} thus obtained are shown as the filled squares in figure 10 and all of these lie close to the QLD/LD curve.

3.3. Other thermodynamic properties

In passing we briefly consider a few further thermodynamic properties. For solid solutions, maxima are frequently observed in the variation of $\Delta C_{p(mix)}$ with temperature (e.g., [28]). For our model system MnO–MgO, $\Delta C_{p(mix)}$ values for any composition show a characteristic maximum at low temperatures (typically $\approx$190 K). The origin is vibrational (rather than configurational) as the maximum is present in the curves for all the separate configurations.

We have also computed, using configurational averaging and the shell model, the variation of the volumetric expansion coefficient, α, and the bulk modulus K_T as a function of composition at 1000 K. α shows positive deviations from that expected from a linear interpolation between the end members with a maximum close to $x_{Mn} \approx 0.9$. K_T shows a negative deviation from linearity. There appear to be little experimental data for oxide solutions for comparison, which is a pity since properties such as α and K_T are key quantities, for example, in geophysical models [29] and our understanding of their variation incomplete.

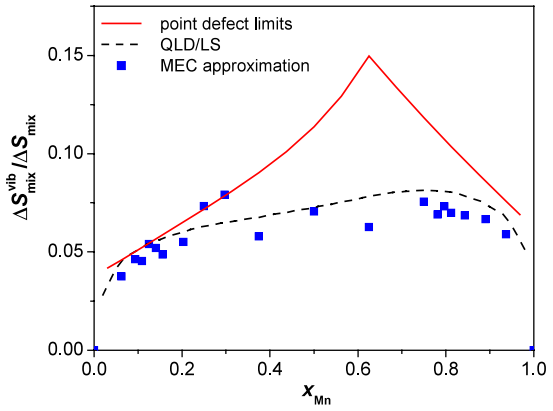

Figure 10. Calculated relative contribution of $\Delta S^{\text{vibr}}_{\text{mix}}$ to ΔS_{mix} for MnO/MgO at 1000 K and zero pressure as a function of composition using combination of configurationally averaged lattice dynamics and configurationally averaged lattice statics (QLD/LS). For comparison purposes, the relative contributions obtained using minimum energy configuration approach (MEC) and the point defect limits (as described in text) are also given.

4. Solid solutions at high pressure

It is straightforward to repeat the calculations for thermodynamic properties at any pressure. To illustrate this we turn to consider the behaviour of the MnO–MgO system at 50 GPa. No phase transitions are expected at this pressure. Neither MnO or MgO undergo a phase transition until the pressure is well in excess of this figure. As earlier we use both configurational averaging and Monte Carlo exchange simulations.

The QLD simulations were carried out using the SHELL code and the same rigid ion model as before with a 128-ion supercell with a face-centred cubic superlattice. Two different sets of 250 randomly chosen configurations were taken into account at given temperature and composition. MCX calculations were carried out as described earlier.

Figure 11 shows calculated values of ΔH_{mix} for MnO/MgO at 50 GPa obtained using QLD and MCX. We see that there is excellent agreement between QLD and MCX. The calculated ΔH_{mix} versus composition curves are symmetric with a maximum of $\approx$4.3 kJ mol^{-1}. A comparison between figures 3 and 11 indicates that ΔH_{mix} decreases with increasing pressure. The variation of ΔH_{mix} with temperature at 50 GPa is even smaller than at zero pressure. The same is true for the vibrational contributions to ΔH_{mix}, which are not only much smaller in magnitude than those at zero pressure but are also now negative rather than positive. This suggests there is a crossover pressure at which the vibrational contributions to ΔH_{mix} are zero.

Figure 12 plots ΔS_{mix} for MnO/MgO at 50 GPa at 1000 K. The temperature dependence is small. Values of ΔS_{mix} obtained using lattice statics (LS), representing the configurational contribution, and also ideal values are shown for comparison. ΔS_{mix} decreases with pressure and at 50 GPa is well below the ideal entropy of mixing, unlike at zero pressure (figure 6(c)). As before, the difference between the QLD and LS results gives the vibrational contributions to ΔS_{mix}, $\Delta S^{\text{vibr}}_{\text{mix}}$, which decreases with increasing pressure, as does the relative contribution of $\Delta S^{\text{vibr}}_{\text{mix}}$ to ΔS_{mix}.

ΔV_{mix} at 50 GPa is given in figure 13. QLD and Monte Carlo values of ΔV_{mix} are now in much better agreement than at zero pressure, and the curves are more symmetric about $x_{\text{Mn}} = 0.5$. Both QLD and MCX indicate ΔV_{mix} increases only slightly with temperature, and less so than at zero pressure. Nevertheless this variation is consistent with the decrease in

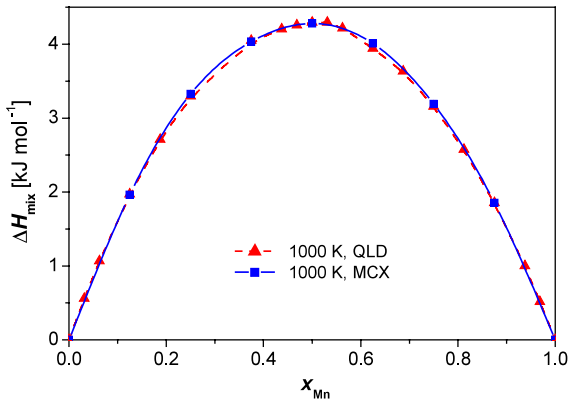

Figure 11. Calculated values of $\Delta H_{\rm mix}$ (kJ mol^{-1}) for MnO–MgO at 50 GPa at 1000 K using configurationally averaged lattice dynamics (QLD) and exchange Monte Carlo (MCX).

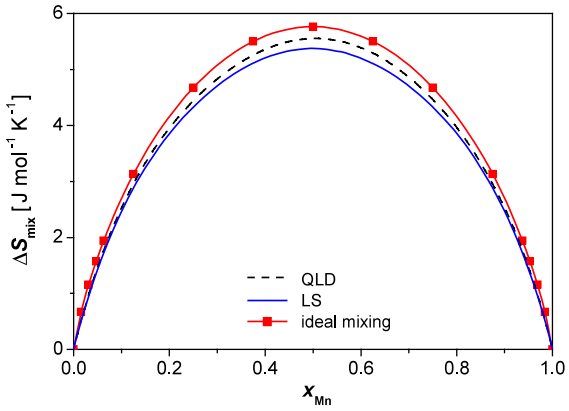

Figure 12. Values of $\Delta S_{\rm mix}$ (J K^{-1} mol^{-1}) for MnO–MgO at 50 GPa and 1000 K as a function of composition. The results from configurational quasiharmonic lattice dynamics (QLD), and configurational averaging using the results of lattice statics minimizations (LS) are shown. Results calculated with QLD and LS. Ideal values are also plotted.

$\Delta S_{\rm mix}$ with pressure, since using a Maxwell relationship,

$$\left(\frac{\partial \Delta V_{\rm mix}}{\partial T}\right)_P = -\left(\frac{\partial \Delta S_{\rm mix}}{\partial P}\right)_T, \tag{11}$$

and also with the decrease in $\Delta H_{\rm mix}$ with pressure, since furthermore

$$\left(\frac{\partial \Delta H_{\rm mix}}{\partial P}\right)_T = \Delta V_{\rm mix} + T\left(\frac{\partial \Delta S_{\rm mix}}{\partial P}\right)_T = \Delta V_{\rm mix} - T\left(\frac{\partial \Delta V_{\rm mix}}{\partial T}\right)_P < 0. \tag{12}$$

Phase diagrams at zero and 50 GPa from QLD, LS and MCX are compared in figures 14(a) and (b). The consolute temperature is predicted to decrease by approximately 150 K and the phase diagram overall to become more symmetric. The agreement between MCX and QLD is better at high pressures than at zero pressure, which presumably reflects the smaller contribution from anharmonic terms at the smaller interionic distances at the higher pressure. The LS phase diagram is also a closer match to that from the full QLD calculation reflecting the smaller role played by the vibrational contributions. This is consistent with the much smaller thermal expansion coefficient at high pressure by a factor of approximately three.

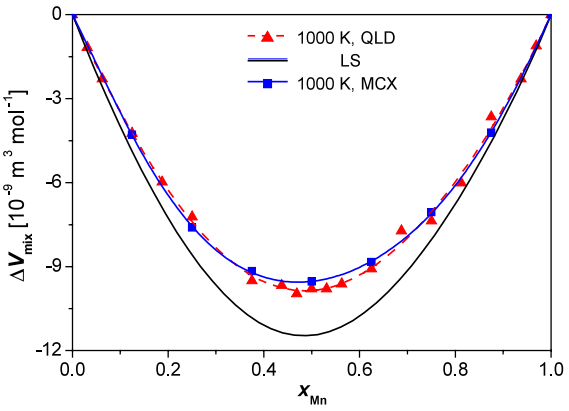

Figure 13. Variation of ΔV_{mix} (10^{-9} m^3 mol^{-1}) for MnO–MgO at 50 GPa with composition. Plots for both 700 and 1000 K are given. Results are from configurational quasiharmonic lattice dynamics (QLD), exchange Monte Carlo (MCX) and configurational averaging using the results of lattice statics minimizations (LS).

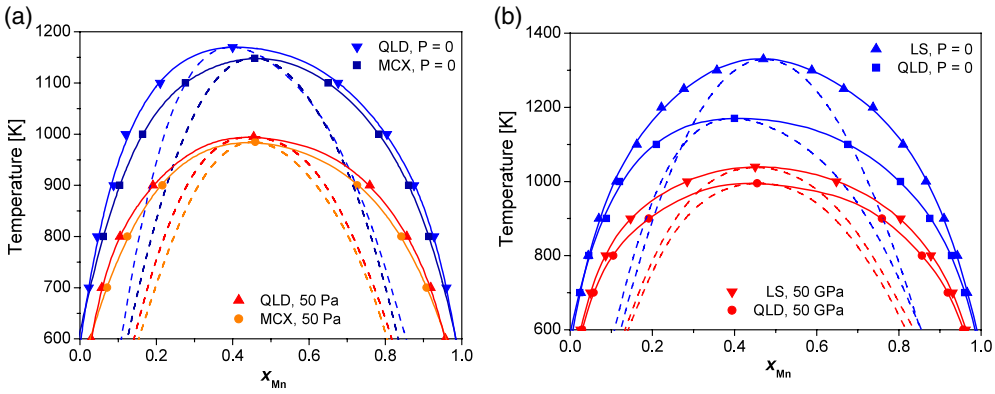

Figure 14. (a) A comparison of calculated phase diagrams (QLD and MCX) of MnO–MgO at 0 and 50 GPa. Consolute temperatures and corresponding compositions are marked in each case. (b) A comparison of calculated phase diagrams (QLD and LS) of MnO–MgO at 0 and 50 GPa. Consolute temperatures and corresponding compositions are marked in each case.

5. Configurational averaging: classifying configurations via radial distribution functions or space group symmetry

Results in previous sections were obtained by forming a thermodynamic average either over all the configurations in a given cell or over a subset chosen at random. In this final section we discuss other methods for selecting configurations.

Our first approach involves the calculation of the Mn–Mn radial distribution function (RDF) for each configuration. We use the radial distribution functions for the purpose of comparison. If two different configurations have the same RDF their unoptimized energies will be the same in a pair potential model. One way to use the RDF is to compare the RDFs of any newly generated configuration with those previously generated. If there is a match we assign the thermodynamic properties of the old configuration to the new one and generate a new configuration.

Table 1. Distinct symmetries, radial distribution functions, static energies and volumes of all arrangements for a 16-ion supercell with a face-centred cubic superlattice for the 50/50 mixture. Radial distribution functions (RDFs) are labelled A, B and C, with the number in parentheses denoting the number of symmetrically distinct configurations with the same RDF.

H, static energy (kJ mol^{-1})	V, volume (10^{-4} m^3 mol^{-1})	N, number of configurations	S, space group (number)	R, type of RDF
−3852.456	1.216 09	8	166	A(2)
−3852.451	1.216 10	8	227	
−3850.701	1.217 20	48	74	B(1)
−3848.946	1.218 31	6	123	C(1)

Alternatively we can find the space group symmetry (SGS) of different configurations and use this information to calculate the number of symmetry-related configurations [30]. Given the space group [31], and the volume of the primitive cell of the configuration we find the total number, N_{total}, of configurations symmetrically equivalent to a given configuration.

If two different configurations have the same relaxed static lattice energy then they have the same space group symmetry. The converse is *not* true; two configurations can have the same space group but different relaxed static energies. As with the RDFs, we can determine the space group of any of the randomly generated configurations, together with the energy, and use this to include the correct weighting of that configuration in the thermodynamic average. We discard configurations subsequently generated if they are symmetrically and energetically equivalent to any already considered.

We illustrate these methods with a 50/50 MnO–MgO mixture, using cells with 16, 32 and 64 ions at 1000 K. The discussion below is restricted to lattice statics (LS) rather than full free energy optimizations of individual configurations. Results are presented from calculations using the random generation, RDF and SGS approaches. The sizes of the two smaller cells allow us also to generate all configurations for comparison. For the largest cell, due to the large number of different configurations ($\approx 6 \times 10^8$), an all configuration calculation is feasible only using the RDF method.

5.1. 16-ion supercell

There are 70 configurations for a 50/50 mixture and this cell size. The calculated free energy at 1000 K using the LS approximation and all configurations in the thermodynamic averaging is −3855.803 kJ mol^{-1}. We see from table 1 that there are *four* sets of configurations each with a different space group, and static lattice energy, but there are only *three* distinct RDFs. Two sets of eight configurations have the same RDF but different optimized lattice energies which differ by 0.005 kJ mol^{-1}. Thus the use of the RDF method and the choice of one configuration per RDF in the averaging leads to only a very small error in H and G of 0.002–0.003 kJ mol^{-1} ($<5.2 \times 10^{-5}$%). This error is negligible for our present purposes. The RDF method is also much faster than any of the other methods due to the rapid comparison of configurations.

5.2. 32-ion supercell

There are now 12 870 configurations for a 50/50 mixture, and we have carried out static energy minimizations on all of them. There are forty sets of configurations, such that the members of each set have the same space group and the same (unrelaxed and relaxed) energy. But there are only seven distinctive RDFs. Configurations may have the same space group but different RDFs and thus different optimized energies, and configurations also exist with the same space

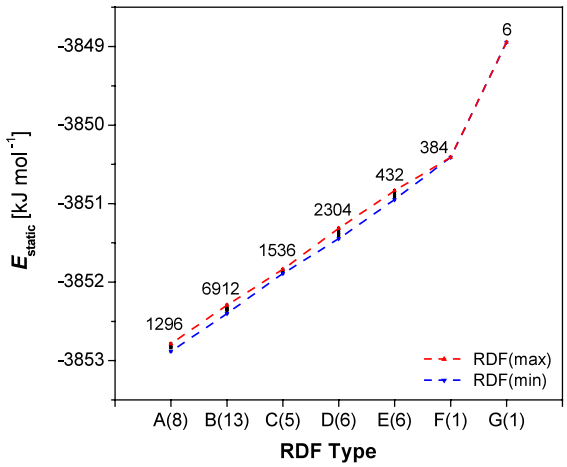

Figure 15. Sketch of the RDF band-like splitting of the calculated energy spectrum of the 50/50 mixture of MnO/MgO at 1000 K using static lattice energies and a supercell containing 32 ions. Mn–Mn RDFs are indicated by a letter and a number in brackets indicating the type of RDF and the total number of different energies for configurations with this type of RDF. Also shown in the plot are the numbers of different configurations having the same RDF. The lines denote the upper (RDF(max)) and the lower limits (RDF(min)) of the different RDF energy bands.

Table 2. Thermodynamic properties of the 50/50 mixture at 1000 K using a 32-ion supercell with a body-centred cubic superlattice, from a calculations using all configurations, and using the RDF method.

Calculation	G (kJ mol^{-1})	H (kJ mol^{-1})	V (10^{-4} m^3 mol^{-1})
All configurations	−3857.191	−3852.426	1.2176
RDF	−3857.194	−3852.428	1.2176
RDF(max)	−3857.142	−3852.377	1.2176
RDF(min)	−3857.244	−3852.479	1.2176

group and RDF but nevertheless different optimized energies. Collected together in table 2 are values of thermodynamic properties of the mixture calculated using all the configurations and the RDF method. The RDF method is by far the most rapid, generating an error of only $\approx$0.003 kJ mol^{-1} ($<1.3 \times 10^{-4}$%) in the calculated value of G at 1000 K.

The separation in energy between configurations with the same RDF is always much smaller than between configurations with different RDFs, as shown graphically in figure 15. Energy splitting between configurations with the same RDFs lead to a set of 'bands'. The narrower the bands, the higher the accuracy of the RDF approach. The maximum spread between of energy in a band, the 'bandwidth', 0.13 kJ mol^{-1}, is negligible compared with the energy range between the maximum and minimum energies of all configurations, 3.94 kJ mol^{-1}.

We can also see from figure 15 the two situations where the RDF algorithm will be most inaccurate. This happens when the randomization in the RDF algorithm generates configurations from each RDF with energies from either only the top or only the bottom of the different energy bands. These two extreme cases are indicated as RDF(min) and RDF(max), in figure 15. The thermodynamic properties of the mixture calculated from these two cases are shown in the last two rows of table 2. We see that the maximum deviation from the correct value of G in these cases is only $\pm$0.05 kJ mol^{-1} ($\pm 1.3 \times 10^{-3}$%). This is so small that it

Table 3. Values of thermodynamic properties of the 50/50 mixture of MnO/MgO at 1000 K using configurationally averaged lattice statics and the 32-ion supercell. For the random and RDF calculations two runs with 1000 configurations generated at random are carried out, as described in the text.

Calculation	G (kJ mol^{-1})	H (kJ mol^{-1})
All configurations	−3857.191	−3852.426
Random(1)	−3857.151	−3852.404
Random(−1)	−3857.148	−3852.402
Random (average)	−3857.150	−3852.403
RDF(1)	−3857.153	−3852.404
RDF(−1)	−3857.188	−3852.419
RDF(average)	−3857.171	−3852.412

justifies the use of the RDF algorithm for larger supercells of MnO/MgO where we are not able to carry out minimizations of all configurations.

How do thermodynamic properties calculated using these methods converge with number of configurations? We have seen that for sufficient convergence of the configurationally averaged properties of the mixture using a cell containing 32 ions, 1000 different arrangements are required if generated at random. We have compared the values from a random based approach with those from calculations using the RDF scheme described above—we compute the RDF of any newly generated configuration and compare it with those for configurations previously generated. If there is a match we assign the thermodynamic properties of the old configuration to the new one. Two runs of configurations generated at random are used. Every run is randomized differently, by a different seed (1 or −1) supplying a random generator which generates different series of configurations. The results of this test after the generation of the first 1000 configurations are listed in table 3. Again it is clear that errors introduced by the both schemes are negligible for the purpose of this paper.

5.3. 64-ion supercell

There are 6.01×10^8 configurations for a 50/50 mixture of MnO–MgO using this cell size. It is not feasible to carry out optimizations for so many configurations! The computer time required for the static optimization of a single configuration is approximately 8 times larger than that for a 32-ion cell and in addition there are more than 46 700 times more configurations that the number for the 50/50 mixture with the 32-ion cell. However, it is feasible to carry out a calculation in which we include one configuration selected at random from each RDF and use the appropriate weighting for that RDF, since there are only 2656 distinct RDFs.

Listed in table 4 are values of thermodynamic properties of the mixture calculated using randomly generated configurations, and by selecting one configuration at random from each set of RDFs. Approximately 450 configurations were required in the previous section for this cell for convergence of ΔG_{mix} to 0.02 kJ mol^{-1}. All the values in table 4 are very close and justify the choice of randomly chosen configurations previously. The RDF procedure is particularly promising for future studies.

6. Final remarks

Solid solutions of ionic compounds have traditionally proved problematic for the theoretician. We have presented a range of methods for the simulation of such solid solutions, the accurate

Table 4. Values of thermodynamic properties of the 50/50 mixture using the 64-ion supercell. For the random (±1) calculations two runs with 1000 configurations generated at random are carried out, as described in the text. The RDF(full (±1)) calculations refer to two sets of calculations in which one configuration is selected at random from each set of RDFs.

Calculation	G (kJ mol^{-1})	H (kJ mol^{-1})
Random(1)	−3857.525	−3852.346
Random(−1)	−3857.538	−3852.352
Random (average)	−3857.532	−3852.349
RDF(full(1))	−3857.527	−3852.351
RDF(full(−1))	−3857.529	−3852.352
RDF(full)(average)	−3857.528	−3852.351

calculation of thermodynamic quantities of mixing, and also for the calculation of phase diagrams. No empirical data are required. All the methods sample many configurations, explicitly considering different arrangements of ions, and allow for the *local* structural relaxation surrounding each cation. This relaxation is crucial. If ignored, the energy of exchange of any two ions is usually very high and all exchanges are rejected, thus sampling only one arrangement. All the methods include vibrational effects and are applicable over ranges of pressure and temperature. Disorder problems are often tackled by using a general Ising model, simplified by limiting interactions to a short range and a finite number of multisite couplings. Such an approach is awkward to parametrize for ionic solids, where relaxation is crucial, and to apply over a range of pressures and temperatures. It is not readily generalized to less symmetric structures, to which we also wish to apply the general methodology outlined here. In our methodology, no assumptions are made as to the nature of the solid solution.

In particular, we have demonstrated how the rapid calculation of the free energy via quasiharmonic lattice dynamics can be used to calculate thermodynamic properties of solutions over wide ranges of pressure and temperature including $\Delta H_{\rm mix}$ and $\Delta S_{\rm mix}$, and phase diagrams. Results compare well with those from Monte Carlo simulations in the semigrand canonical ensemble, and the agreement is better at higher pressure where internuclear distances are smaller and anharmonic contributions smaller. Quantum effects are included in the vibrational contributions at low temperatures. Calculated entropies of mixing include *both* configurational and vibrational contributions. For the latter we have seen when extrapolation from the point defect limit fails. The technique is limited only by the accuracy of the quasiharmonic approximation, which breaks down with increasing amplitude of vibration and hence at high T, typically around two thirds of the melting point for oxides. Randomly generated configurations have been sufficient for the properties considered in this paper. Use of space group information is of course essential for finding the number of all symmetrically equivalent configurations to one configuration which will be essential for more non-ideal solutions than that considered here. Since different configurations may have the same space group symmetry but very different energies, in our method we still need to optimize every configuration in turn to establish whether a newly generated configuration has already been optimized. Different configurations can be compared rapidly by computing their RDF. The RDF method is not exact since there may be symmetrically non-equivalent configurations with the same RDF. However, in the example here this leads to only very small inaccuracies in the thermodynamic averages. Overall the striking success of the RDF method is very encouraging.

The Monte Carlo and the configurational averaging methods each have their own strengths and advantages. Monte Carlo techniques are applicable to the solid at high temperatures and to

melts [20]. The semigrand canonical ensemble is an attractive route to differences in chemical potential and consequent calculation of the free energy and the phase diagram. Further work is in progress to develop all of the methods and apply them to more complicated systems, including much more complex mineral structures such as garnets and also highly non-ideal examples, such as oxygen-deficient perovksites [32].

Acknowledgments

This work was funded by EPSRC grants GR/M53899, GR/R85952 and an ORS award to ITT. It has also been supported by Norsk Forskningsråd (project number 142995/432) and a grant of computing time from the Research Council of Norway Supercomputing Programme. Computational facilities were made available through two JREI HEFCE grants. Help from Hugh Barron is gratefully acknowledged.

References

[1] de Fontaine D 1994 *Solid State Phys.* **47** 33
[2] e.g. Catlow C R A and Mackrodt W C 1982 *Computer Simulation of Solids* ed C R A Catlow and W C Mackrodt (Berlin: Springer) chapter 1
[3] Norgett M J 1974 *Harwell Report* AERE-R 7650, AEA Technology Harwell Laboratory, Didcot, Oxon OX11 0RA
[4] e.g. Taylor M B, Barrera G D, Allan N L, Barron T H K and Mackrodt W C 1997 *Faraday Discuss.* **106** 377
[5] Taylor M B, Barrera G D, Allan N L, Barron T H K and Mackrodt W C 1998 *Comput. Phys. Commun.* **109** 135
[6] Taylor M B, Barrera G D, Allan N L and Barron T H K 1997 *Phys. Rev.* B **56** 14380
[7] Sanchez J M, Ducastelle F and Gratias D 1984 *Physica* A **128** 334
[8] Zunger A, Wei S-H, Ferreira L G and Benard J E 1990 *Phys. Rev. Lett.* **65** 353
[9] van der Walle A and Ceder G 2002 *Rev. Mod. Phys.* **74** 11
[10] McCormack R and Burton B P 1997 *Comput. Mater. Sci.* **8** 153
[11] Burton B P and van der Walle A 2003 *Phys. Chem. Minerals* **30** 88
[12] Kofke D A and Glandt E D 1988 *Mol. Phys.* **64** 1105
[13] Frenkel D and Smit B 2002 *Understanding Molecular Simulation* 2nd edn (San Diego, CA: Academic)
[14] Marquez F M, Cienfuegos C, Pongsai B K, Lavrentiev M Yu, Allan N L, Purton J A and Barrera G D 2003 *Modelling Simul. Mater. Sci. Eng.* **11** 115
[15] de Villiers J P R, Buseck P R and Steyn H S 1998 *Miner. Mag.* **62** 333
[16] Raghavan S, Iyengar G N K and Abraham K P 1985 *J. Chem. Thermodyn.* **17** 585
[17] Wood B J, Hackler R T and Dobson D P 1994 *Contrib. Mineral Petrol.* **115** 438
[18] Allan N L, Barrera G D, Fracchia R M, Lavrentiev M Yu, Taylor M B, Todorov I T and Purton J A 2001 *Phys. Rev.* B **63** 094203
[19] Allan N L, Barrera G D, Lavrentiev M Yu, Todorov I T and Purton J A 2001 *J. Mater. Chem.* **11** 63
[20] Lavrentiev M Yu, Allan N L, Barrera G D and Purton J A 2001 *J. Phys. Chem.* B **105** 3594
[21] Metropolis N I, Rosenbluth A W, Rosenbluth M N, Teller A H and Teller E 1953 *J. Chem. Phys.* **21** 1087
[22] Lewis G V and Catlow C R A 1985 *J. Phys. C: Solid State Phys.* **18** 1149
[23] Dick B G and Overhauser A W 1958 *Phys. Rev.* **112** 90
[24] Gripenberg H, Seetharaman S and Staffansson L I 1978–79 *Chem. Scr.* **13** 162
[25] Raghavan S 1971 *PhD Thesis* Indian Institute of Science, Bangalore
[26] e.g. Thompson J B 1967 *Researches in Geochemistry* vol 2, ed P H Abelson (New York: Wiley) p p 340
[27] Allan N L, Barron T H K and Bruno J A O 1996 *J. Chem. Phys.* **105** 8300
[28] Geiger C A (ed) 2001 *European Mineralogical Union Notes in Mineralogy* vol 3 *Solid Solutions in Silicate and Oxide Systems* series eds G Papp and T G Weiszburg (Budapest: Eötvös University Press) chapter 4
[29] e.g. Anderson O L 1995 *Equations of State of Solids for Geophysics and Ceramic Science* (Oxford: Oxford University Press)
[30] Barron T H K, private communication
[31] Le Page Y 1987 *J. Appl. Crystallogr.* **20** 264
[32] Bakken E, Allan N L, Barron T H K, Mohn C E, Todorov I T and Stølen S 2003 *Phys. Chem. Chem. Phys.* **5** 2237